Open access • Journal Article • DOI:10.1109/JSEN.2004.841343

Microwave polarimetry tomography of wood — Source link

Anders Kaestner, Lars B. Bååth

Institutions: ETH Zurich, Halmstad University

Published on: 04 Apr 2005 - IEEE Sensors Journal (IEEE)

Topics: Polarimetry and Microwave imaging

Microwave polarimetry tomography of wood

Anders P. Kaestner and Lars B. Bååth

Kaestner A, Bååth L. Microwave polarimetry tomography of wood. IEEE; IEEE Sensors Journal. 2005;5(2):209-215.

DOI: 10.1109/JSEN.2004.841343

Microwave Polarimetry Tomography of Wood

Anders P. Kaestner and Lars B. Bååth

***Abstract*—In this paper, we present a new microwave-based method to make images of fiber structure, e.g., to locate knots in wood. Evaluation of Maxwell's equations for an electromagnetic wave propagating in an anisotropic media (wood) shows that the polarization of the wave depends on the local fiber orientation in the sample. Experiments support the theoretical evaluation showing that knots can be followed in images of polarimetric parameters, reconstructed from multiple monostatic measurements. The equipment works at low intensity and is, therefore, virtually harmless to human beings; furthermore, it can be made portable and be operated by a single person.**

***Index Terms*—Microwaves, noninvasive testing, polarimetry, tomography, wood.**

I. Introduction

SCANNING wood for the internal structure has been of large interest in research during the past ten years. The reasons for the interest are the possibility to determine the quality of standing trees in the forest as well as the quality of the delivered timber. In addition to the quality measurements, there is also the task of optimizing the cutting strategy and lumber grading.

Various approaches to solve these tasks have been suggested, e.g., Schmoldt *et al.* [1] used ultrasound for lumber grading. The ultrasound technique is, however, not a very good choice for online applications, since it depends on good contact with the measured object as well as being sensitive to mechanical vibration harmonics in the plant. The most common approach is to use X-ray-based technology (Lee *et al.* [2], Svalbe *et al.* [3], Zhu *et al.* [4]). This approach usually produces high-quality images of the inner structure and therefore the emphasis of the research is on image analysis. Studies of the interaction between wood and X-rays have also been made by Oja and Temnerud [5]. The disadvantages of X-ray-based systems include high cost, dangerous radiation, and the equipment is often too slow to be used in a real-time sawmill application.

As an alternative to the two previously mentioned methods, we propose the use of a scanning device based on polarized microwaves. Using microwaves for wood scanning is a recent approach and, usually, the measurements are only based on measuring the properties of the transmitted wave at a single frequency or alternatively using pulse radar-based systems. Previously published approaches have concentrated on two areas of microwave measurements:

1) **Detections of defects** have been made by studying phase changes and attenuation of electromagnetic waves at single frequencies (Choffel *et al.* [6], King [7], Forrer and Funck [8]).
2) Methods for **measurements of moisture, density, and grain angle** have been presented by James *et al.* [9], Tiuri *et al.* [10], and Belenkii and Taibin [11]. Finally, Shen [12] used the depolarization as a measure of the grain angle of sawn boards.

The aim of our approach is to detect defects and variations in wood based on measurements giving information about grain angle, moisture content, and density. This information is contained in the dielectric tensor. As a first step, we measure the depolarization of the reflected field. The depolarization is the effect of variations in the spatial distribution of the dielectric tensor. In this paper, we describe the background theory and the technology needed to study the spatial distribution of the fiber structure of wood.

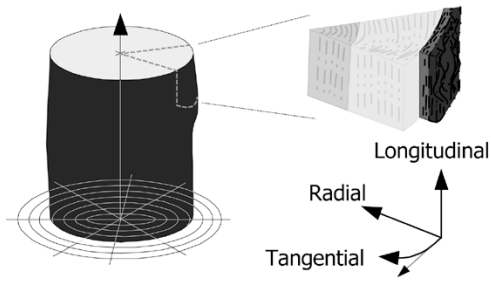

Fig. 1. Defining the coordinate system of a log and showing the principal directions of the anisotropy.

II. Theory

This section is divided into two parts: describing the material properties of wood and the electromagnetic propagation in wood as a dielectric medium [13], followed by an example to demonstrate our measurement technology.

A. Propagation in Wood

Wood is a dielectrically anisotropic medium with the principal axes in the following directions: tangential to the annual ring, parallel to the fibers, and radial from the center of growth, as shown in Fig. 1. The natural coordinate system of a tree is cylindrical with two orthogonal Euclidean dimensional axes: one following the general growth of the tree and another pointing outwards from the central axis. The third axis is non-Euclidean and follows the general curvature of the annual rings of the tree. For the purpose of this paper, we introduce

Manuscript received December 30, 2003; revised August 27, 2004. This work was supported by the program for Visual Information Technology (VISIT) of the Swedish Foundation for Strategic Research. The associate editor coordinating the review of this paper and approving it for publication was Dr. Krikor Ozanyan.

A. P. Kaestner is with the Institute for Terrestrial Ecology, ETH Zurich, CH-8952 Schlieren, Switzerland (e-mail: anders.kaestner@env.ethz.ch).

L. B. Bååth is with the Electronics and Physics Laboratory, School of Information Science, Computer, and Electrical Engineering, Halmstad University, S-301 18 Halmstad, Sweden (e-mail: lars.baath@ide.hh.se).

Digital Object Identifier 10.1109/JSEN.2004.841343

local observational Euclidean and Cartesian coordinate systems, with origin at the circumference of the tree. Each system is rotated a defined angle to the others and all have the same origin position offset as to the center of the tree growth. The local radial axis is pointing inwards in the direction of the transmitted wave (negative z direction, as referenced to the natural system of the tree); the second local axis is along the natural growth direction and the third local axis is locally approximated as the tangent of the circumference in the coordinate origin point. This is motivated by the effective target surface of the sample, which is so small that the interface can be approximated to be a plane. Furthermore, since only a narrow fraction of the transmitted wave is actually measured, we approximate it to be a plane wave. With these approximations, we see it motivated to analyze the propagation in a local observational Cartesian coordinate system and modeling the propagation problem as a plane wave in discrete anisotropic media.

The origin of the anisotropy is the combined results from the molecular structure of cellulose up till the fiber structure in the wood [14]. The dielectric tensor has only dielectric constants in the three principal directions along the diagonal in the matrix as

$$\boldsymbol{\epsilon}'(\omega) = \begin{pmatrix} \epsilon_T(\omega) & 0 & 0 \\ 0 & \epsilon_L(\omega) & 0 \\ 0 & 0 & \epsilon_R(\omega) \end{pmatrix}. \tag{1}$$

ϵ_L is the dielectric constant along the longitudinal direction, i.e., parallel to the fibers, ϵ_R the radial, and ϵ_T the tangential. The directions are given relative to the annular rings and the fiber direction of a log. The relation between the diagonal elements is $\epsilon_T \leq \epsilon_R < \epsilon_L$, but since $\epsilon_R \approx \epsilon_T$, they are approximated as ϵ_{RT} in the following evaluation. The ratio ϵ_L/ϵ_{RT} varies with frequency and moisture content (MC), e.g., $\epsilon_L/\epsilon_{RT} = 1.1$–$1.8$ for MC $= 5$–100% for the considered frequencies [15]. Wood is also a nonmagnetic material and, thus, the permeability become

$$\boldsymbol{\mu} = \mu_0 \mathbf{I}$$

i.e., independent of the orientation of the medium.

The dielectric matrix in (1) describes the local properties in the material where the orientations are aligned according to the principal directions of wood as showed with the slice to the right in Fig. 1. If, however, the orientation of the wave differs from the local orientation of the fibers in the log, then the field is modified by a two-angle rotation

$$\boldsymbol{\epsilon} = \mathbf{R}^T \boldsymbol{\epsilon}' \mathbf{R} \tag{2}$$

where ϵ' represent the dielectric matrix in local coordinates and ϵ is given in the local observing coordinates and

$$\mathbf{R} = \begin{pmatrix} \sin\beta & -\cos\beta & 0 \\ \cos\alpha\cos\beta & \cos\alpha\sin\beta & -\sin\alpha \\ \sin\alpha\cos\beta & \sin\alpha\sin\beta & \cos\alpha \end{pmatrix}$$

is a rotation matrix rotating the local coordinate system to match the local observing coordinate system. The rotation angles α and β of R are as shown in Fig. 2, resulting in the matrix perceived by the wave.

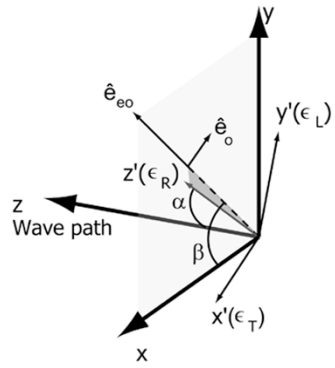

Fig. 2. Local coordinate system (oriented with the local fiber direction) related to the local Cartesian observational coordinate system (the wave propagates along the z axis).

The wave is transmitted from z_0 as a plane wave traveling in the positive z direction with the components, i.e.

$$\boldsymbol{E}(z_0,\omega) = \begin{pmatrix} E_x(z_0,\omega) \\ E_y(z_0,\omega) \\ 0 \end{pmatrix} \quad \boldsymbol{H}(z_0,\omega) = \begin{pmatrix} H_x(z_0,\omega) \\ H_y(z_0,\omega) \\ 0 \end{pmatrix}. \tag{3}$$

Maxwell's equations for a plane wave along a fixed direction (z axis) are

$$\begin{aligned} \nabla \times \boldsymbol{E}(z,\omega) &= j\omega \boldsymbol{B}(z,\omega) \\ \nabla \times \boldsymbol{H}(z,\omega) &= -j\omega \boldsymbol{D}(z,\omega) \end{aligned} \tag{4}$$

due to the properties of wood, the constitutive relations of D and B become

$$\begin{aligned} \boldsymbol{D}(z,\omega) &= \epsilon_0 \boldsymbol{\epsilon}(z,\omega) \boldsymbol{E}(z,\omega) \\ \boldsymbol{B}(z,\omega) &= \frac{1}{c_0} \eta_0 \mu_0 \boldsymbol{H}(z,\omega). \end{aligned} \tag{5}$$

Observe that the dielectric tensor here has a spatial and orientational dependency in the z direction. The spatial dependency has two main origins. First, the local fiber orientation is not constant over the cut. Secondly, the dielectric properties are not constant due to different properties in sapwood and heartwood and local variations in moisture content.

Only the z derivatives have to be considered for the solution of (4), since there are no contributions from the other directions. Maxwell's equations, therefore, can be reduced to (the coordinate z and the frequency ω are implied in the rest of the evaluation)

$$\frac{d}{dz} \begin{pmatrix} \boldsymbol{E}_{xy} \\ \eta_0 \boldsymbol{H}_{xy} \end{pmatrix} = j\omega \begin{pmatrix} -\mathbf{J} & 0 \\ 0 & \mathbf{J} \end{pmatrix} \begin{pmatrix} \boldsymbol{B}_{xy} \\ \eta_0 \boldsymbol{D}_{xy} \end{pmatrix} \tag{6}$$

where

$$\mathbf{J} = \begin{pmatrix} 0 & -1 \\ 1 & 0 \end{pmatrix}$$

is a rotational operator. The dielectric tensor can be written as

$$\boldsymbol{\epsilon} = \left(\begin{array}{c|c} \boldsymbol{\epsilon}_{\perp\perp} = \begin{pmatrix} \epsilon_{11} & \epsilon_{12} \\ \epsilon_{21} & \epsilon_{22} \end{pmatrix} & \boldsymbol{\epsilon}_{\perp} = \begin{pmatrix} \epsilon_{13} \\ \epsilon_{23} \end{pmatrix} \\ \hline \boldsymbol{\epsilon}_z = \begin{pmatrix} \epsilon_{31} & \epsilon_{32} \end{pmatrix} & \boldsymbol{\epsilon}_{zz} = \epsilon_{33} \end{array} \right)$$

where ϵ_{nm}, representing the elements of (2). $\boldsymbol{\epsilon}$ is symmetric and, thus, $\boldsymbol{\epsilon}_z = \boldsymbol{\epsilon}_\perp^T$. The dielectric tensor is divided into two parts (one considering the xy components and the other the z components) and the xy components in (5) can be written as

$$\begin{aligned} D_{xy} &= \epsilon_0 \left(\boldsymbol{\epsilon}_{\perp\perp} \cdot \boldsymbol{E}_{xy} + \boldsymbol{\epsilon}_\perp E_z\right) \\ B_{xy} &= \frac{\eta_0}{c_0} \left(\boldsymbol{\mu}_{\perp\perp} \cdot \boldsymbol{H}_{xy} + \boldsymbol{\mu}_\perp H_z\right). \end{aligned} \tag{7}$$

Inserting (7) into (6), this becomes

$$\begin{aligned} \frac{d}{dz}\begin{pmatrix} \boldsymbol{E}_{xy} \\ \eta_0 \boldsymbol{H}_{xy} \end{pmatrix} = j\frac{\omega}{c_0}\begin{pmatrix} -\mathbf{J} & 0 \\ 0 & \mathbf{J} \end{pmatrix} \\ \times \begin{pmatrix} \eta_0 \left(\boldsymbol{\mu}_{\perp\perp} \cdot \boldsymbol{H}_{xy} + \boldsymbol{\mu}_\perp H_z\right) \\ \boldsymbol{\epsilon}_{\perp\perp} \cdot \boldsymbol{E}_{xy} + \boldsymbol{\epsilon}_\perp E_z \end{pmatrix} \end{aligned} \tag{8}$$

the z components of $\nabla \times \boldsymbol{E}$ and $\nabla \times \boldsymbol{H}$ are both equal to zero since the considered wave is only propagating along the z direction, thus

$$\begin{cases} D_z = \boldsymbol{\epsilon}_z \cdot \boldsymbol{E}_{xy} + \epsilon_{zz} E_z = 0 \\ B_z = \boldsymbol{\mu}_z \cdot \boldsymbol{H}_{xy} + \mu_{zz} H_z = 0 \end{cases}$$

which gives

$$E_z = -\frac{\boldsymbol{\epsilon}_z \cdot \boldsymbol{E}_{xy}}{\epsilon_{zz}} \qquad H_z = -\frac{\boldsymbol{\mu}_z \cdot \boldsymbol{H}_{xy}}{\mu_{zz}}. \tag{9}$$

Using the z components given by (9) in (8), it can be rewritten as

$$\frac{d}{dz}\begin{pmatrix} \boldsymbol{E}_{xy} \\ \boldsymbol{H}_{xy} \end{pmatrix} = j\frac{\omega}{c_0}\mathbf{W}\begin{pmatrix} \boldsymbol{E}_{xy} \\ \boldsymbol{H}_{xy} \end{pmatrix} \tag{10}$$

where $\mathbf{W}$ is a coefficient matrix that in our case is defined as

$$\mathbf{W} = \begin{pmatrix} 0 & -\mu\mathbf{J} \\ -\mathbf{J} \cdot \boldsymbol{\epsilon}_{\perp\perp} - \frac{\mathbf{J} \cdot \boldsymbol{\epsilon}_\perp \boldsymbol{\epsilon}_z}{\epsilon_{zz}} & \mathbf{0} \end{pmatrix}.$$

The solution to (10), which is a system of ordinary differential equations, can be obtained as the eigenvalues of the coefficient matrix $\mathbf{W}$

$$\begin{cases} l_1 = -l_2 = (\epsilon_{RT}\mu_0)^{1/2} \\ l_3 = -l_4 = \left(\mu_0 \frac{\epsilon_L \epsilon_{RT}}{\epsilon_{33}}\right)^{1/2}. \end{cases} \tag{11}$$

The branch of the root is chosen such that the imaginary part is nonnegative. The latter two eigenvalues l_3 and l_4 depend on the media orientation due to $\epsilon_{33} = \epsilon_L \cos^2\alpha + \epsilon_{RT} \sin^2\alpha$ in the denominator. The eigenvalues in (11) only depend on the angle α because of axial symmetry around the z axis. The eigenvalues of the solution are related to the wave number in the medium as

$$\begin{cases} k_o = l_o k_0 \\ k_{eo} = l_{eo} k_0 \end{cases}. \tag{12}$$

The corresponding eigenvectors of the solution ($\hat{\boldsymbol{e}}_o$ and $\hat{\boldsymbol{e}}_{eo}$) are related to the $\hat{\boldsymbol{x}}$ and $\hat{\boldsymbol{y}}$ axes as

$$\begin{pmatrix} \hat{\boldsymbol{e}}_o \\ \hat{\boldsymbol{e}}_{eo} \end{pmatrix} = \begin{pmatrix} \cos\beta & -\sin\beta \\ \sin\beta & \cos\beta \end{pmatrix}\begin{pmatrix} \hat{\boldsymbol{x}} \\ \hat{\boldsymbol{y}} \end{pmatrix} \tag{13}$$

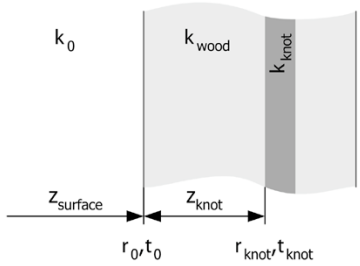

Fig. 3. Approximating the log by piecewise homogeneous layers.

and the resulting field solutions relative to the local coordinates become

$$\begin{aligned} \boldsymbol{E}^o_{xy}(z,\omega) &= E_o(\omega)\hat{\boldsymbol{e}}_o e^{\pm jk_o z} \\ \boldsymbol{E}^{eo}_{xy}(z,\omega) &= E_{eo}(\omega)\hat{\boldsymbol{e}}_{eo} e^{\pm jk_{eo} z} \end{aligned} \tag{14}$$

i.e., two solutions are available and propagating in the positive and negative $\hat{z}$ directions. As a consequence of this solution will the state of polarization be altered by the orientation of the sample. The polarization is altered at a point in the fiber material, i.e., wood, as follows.

1) The axial ratio ϵ_L/ϵ_{RT} of the dielectric matrix is directly related to the density and the moisture content of the material. This ratio is the amount of polarization altered at this point.
2) The fiber position angle (β) in the longitudinal–tangential plane determines the linear tilt angle of the polarization.
3) The radial fiber angle (α) is mainly responsible for the degree of elliptical polarization.

B. Basic Principle of the Measurements

In our measurements, we transmit a linearly polarized E field tilted to $\tau = 45°$; the complete transmitted field can be written as

$$\boldsymbol{E}_{xy} = \begin{pmatrix} E_x \\ E_y \end{pmatrix} = \begin{pmatrix} E_0 \\ E_0 \end{pmatrix} e^{j\omega t}. \tag{15}$$

We will, for simplicity, discuss in the following a simple case with only two layers of wood structure. The trunk is in this example approximated by a layered medium (Fig. 3), where each layer corresponds to a plane parallel to the plane formed by the x and y axes. The layers are furthermore considered to be homogeneous with wave numbers

$$\mathbf{k}_0 = k_0 \begin{pmatrix} 1 & 0 \\ 0 & 1 \end{pmatrix} \tag{16}$$

for air and

$$\mathbf{k}_{\text{medium}} = \begin{pmatrix} k^o_{\text{medium}} & 0 \\ 0 & k^{eo}_{\text{medium}} \end{pmatrix} \tag{17}$$

for propagation in wood; media is replaced by the corresponding part of the tree (wood and knot). The field incidence is normal to the plane of the layers.

The indices of refraction used to form the admittance matrices are defined as the eigenvalues in (11); thus, the admittances for the three layers become

$$\mathbf{Y}_0 = \begin{pmatrix} 0 & \frac{-1}{\eta_0} \\ \frac{1}{\eta_0} & 0 \end{pmatrix} \tag{18}$$

$$\mathbf{Y}_{\text{medium}} = \begin{pmatrix} 0 & -n^{o}_{\text{medium}} \\ n^{eo}_{\text{medium}} & 0 \end{pmatrix} \tag{19}$$

where η_0 is the intrinsic impedance of air and n_{medium} are the indices of refraction for the ordinary and extraordinary waves in different parts of the medium, i.e., wood and knot. These matrices are used to compute the reflection matrices as

$$\mathbf{r}_{\text{surface}} = (\mathbf{Y}_{\text{wood}} + \mathbf{Y}_0)^{-1}(\mathbf{Y}_{\text{wood}} - \mathbf{Y}_0) \tag{20}$$

for the first interface and

$$\mathbf{r}_{\text{knot}} = (\mathbf{Y}_{\text{knot}} + \mathbf{Y}_{\text{wood}})^{-1}(\mathbf{Y}_{\text{knot}} - \mathbf{Y}_{\text{wood}}) \tag{21}$$

for the second interface. Explicitly, (20) and (21) become

$$\mathbf{r}_{\text{surface}} = \frac{1}{(n^{o}_{\text{wood}} + n_0)(n^{eo}_{\text{wood}} + n_0)} \times \begin{pmatrix} {n^{o}_{\text{wood}}}^2 - {n_0}^2 & 0 \\ 0 & {n^{eo}_{\text{wood}}}^2 - {n_0}^2 \end{pmatrix} \tag{22}$$

and

$$\mathbf{r}_{\text{knot}} = \frac{1}{(n^{o}_{\text{knot}} + n^{o}_{\text{wood}})(n^{eo}_{\text{knot}} + n^{eo}_{\text{wood}})} \times \begin{pmatrix} {n^{o}_{\text{knot}}}^2 - {n^{o}_{\text{wood}}}^2 & 0 \\ 0 & {n^{eo}_{\text{knot}}}^2 - {n^{eo}_{\text{wood}}}^2 \end{pmatrix} \tag{23}$$

where n^{o}_{medium} and n^{eo}_{medium} are the indices of refraction the ordinary and extraordinary waves, respectively, in the trunk and knot. The transmission matrix from the first interface is also needed for the example

$$\mathbf{t}_{\text{surface}} = \mathbf{I} - \mathbf{r}_{\text{surface}}. \tag{24}$$

These matrices show that interface transitions only are affected by the angle α. The fields at the interfaces are related to the local coordinate system and must, thus, be rotated by the rotation operation

$$E^{\text{global}}_{\text{interface}} = \mathbf{R}^{-1}(\beta_{\text{medium}})E^{\text{local}}_{\text{interface}} \tag{25}$$

with $\mathbf{R}(\beta_{\text{medium}})$ as the rotation matrix in (13).

The reflected field of the log consists of the sum of the reflections from the surface and the from the knot. Thus, the received field at the antenna becomes

$$\boldsymbol{E}^{xy}_{\text{receive}}(\omega) = \mathbf{R}^{-1}(\beta_{\text{wood}})\boldsymbol{E}_{\text{surface}}(\omega) + \mathbf{R}^{-1}(\beta_{\text{knot}})\boldsymbol{E}_{\text{knot}}(\omega). \tag{26}$$

The overall geometry of the sample is aligned such that the angle β_{wood} can be considered to be equal to zero. To reduce the complexity of the expressions are only the reflections from the front surface and the front of the knot considered; to be more correct, there the reflections from the backside of the knot as well as the log that should also be included. The two terms in (26) are the field contribution from the surface reflection

$$\boldsymbol{E}_{\text{surface}}(\omega) = \mathbf{r}_{\text{surface}}\boldsymbol{E}_{xy}(\omega)e^{j(2\mathbf{k}_0 z_{\text{surface}})} \tag{27}$$

while the knot reflection results in a field as

$$\boldsymbol{E}_{\text{knot}}(\omega) = \mathbf{t}_{\text{surface}}\mathbf{r}_{\text{knot}}\mathbf{t}_{\text{surface}} \cdot \boldsymbol{E}_{xy}(\omega)e^{j(2\mathbf{k}_0 z_{\text{surface}} + 2\mathbf{k}_{\text{wood}} z_{\text{knot}})}. \tag{28}$$

The received signal has a temporal coherence with the transmitted signal, a property used by the hardware that only extracts signals that correlate with the transmitted. This approach is very insensitive to noise and can, thus, register weak signals in the presence of noise. This is the reason why we can work at low intensity.

Equation (26) is describing only the signal at the frequency ω which is insufficient to resolve multiple spatial variations. This limitation can be overcome by sampling a discrete frequency spectrum in the interval $[\omega_{lo}, \omega_{hi}]$ followed by an inverse Fourier transform into a time-delay spectrum. By selecting the time interval of the Fourier transform $t \in [t_1, t_2]$, the time delay can be computed for a region of interest. The time delay can be converted into propagation distances by the relation $d = ct$ where c is the speed of electromagnetic propagation in the medium. The transformed signal $f[t]$ or $f[d]$ shows the spatial distribution of the E field, or, as in our case, the intensity of the E field.

The time-delay spectrum shows intensity peaks at the the locations of the interfaces. Unfortunately, the reflections inside the log are weak and, thus, difficult to identify. The internal reflections in the sample are weak due to a combination of two factors.

1) A quite large fraction of the field is reflected and scattered from the first surface leaving a small part to propagate through an attenuating medium.
2) The spatial variations of the dielectric tensor inside the medium are small, unless an artefact is present.

Since it is hard to find anything but the surface reflection using the intensity, we study the spatial distribution of polarization related parameters.

A measurement contains reflections from all reflecting objects in the surroundings that add up to the measured signal due to superposition. This background clutter is undesired, since it often has amplitudes larger than the signal we intend to measure, i.e., our signal disappears in the clutter. To remove the clutter, we consider the background to be static. After this assumption, the clutter can be removed by subtracting a background reference spectrum from the wood measurement as

$$\boldsymbol{E}_{\text{wood}}(\omega) = \boldsymbol{E}_{\text{receive}}(\omega) - \boldsymbol{E}_{\text{clutter}}(\omega). \tag{29}$$

C. Polarimetric Calculations

The polarization calculations are based on the two measured field components $E_{\parallel}$ and $E_{\perp}$ in the time domain. The simplest relation to identify the presence of depolarization is the quotient between the received power from the two linearly polarized waves $E_{\perp}$ and $E_{\parallel}$ according to

$$\rho = \frac{E_{\parallel}}{E_{\perp}}. \tag{30}$$

This polarization ratio is a complex valued quantity. To analyze the polarization ratio, it is first separated into two real-valued quantities which are interesting to study: namely, the amplitude ($|\rho|$) and the argument ($\gamma = \arg(\rho)$). If $|\rho|$ deviates from unity, a depolarization is present, since the two emitted waves were

Fig. 4. Photo of the arrangement.

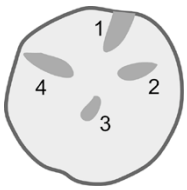

Fig. 5. Geometry of the measured slice; the numbers label the knots.

of equal intensity. The same applies to γ, for which a deviation from zero indicates a depolarization, since the transmitter originally emits the two waves at the same phase.

The polarization of the field can be described with the Stoke parameters, as the correlation of the field components $E_{\|}$ and $E_{\perp}$ combined as

$$\begin{aligned} I &= E_{\|}E_{\|}^{*} + E_{\perp}E_{\perp}^{*} \\ Q &= E_{\|}E_{\|}^{*} - E_{\perp}E_{\perp}^{*} \\ U &= E_{\|}E_{\perp}^{*} + E_{\perp}E_{\|}^{*} \\ V &= -j(E_{\|}E_{\perp}^{*} - E_{\perp}E_{\|}^{*}) \end{aligned} \tag{31}$$

where $(^{*})$ denotes the complex conjugate of the quantity. The first Stoke parameter (I) describes the total intensity of the wave and contains both polarized power and unpolarized power in contrast to the remaining three parameters which only contain the polarized part of the wave.

Normalizing the Stoke parameters with respect to the first parameter I results in the normalized Stoke parameters which relate to the angles (ε and τ) of the state of polarization as

$$\begin{aligned} s_0 &= 1 \\ s_1 &= d\cos 2\varepsilon \cos 2\tau \\ s_2 &= d\cos 2\varepsilon \sin 2\tau \\ s_3 &= d\sin 2\varepsilon \end{aligned} \tag{32}$$

1) The ellipticity angle (ε) describes the phase difference between the two field components $E_{\|}$ and $E_{\perp}$. This quantity also describes the degree of elliptical polarization. The value of ε for an unaffected wave transmitted from our system should be equal to zero, since the considered transmitted wave is completely linearly polarized, i.e., the two waves have the same phase.

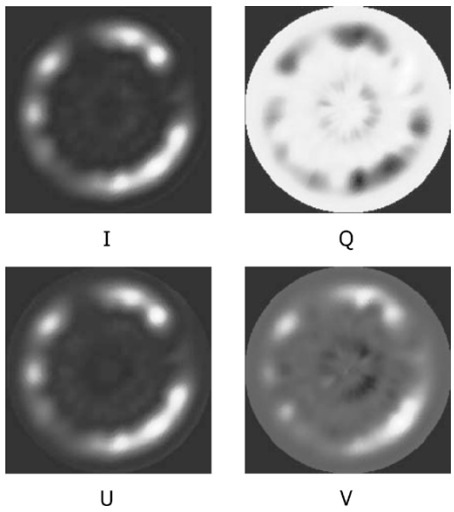

Fig. 6. Slice images showing the distribution of the Stoke parameters (I, Q, U, and V) in a piece of spruce.

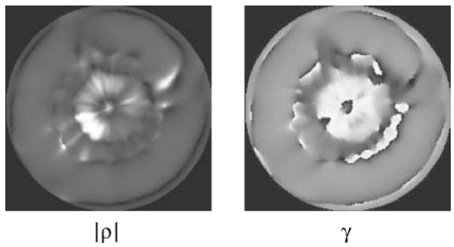

Fig. 7. Slice images showing the polarization ratio ρ as amplitude $|\rho|$ and angle γ in a piece of spruce.

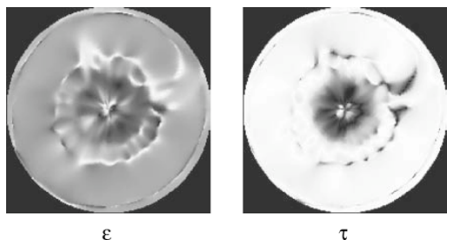

Fig. 8. Slice images of the angles describing the state of polarization (ε: ellipticity; τ: linear tilt).

2) The second variable (τ) describes the angle between the two field components $E_{\|}$ and $E_{\perp}$, and, thus, describes the tilt of the linear polarization, called the linear tilt angle. In our case, we emit $E_{\|}$ and $E_{\perp}$ at equal phase and amplitude [see (15)] resulting in a completely linearly polarized wave with a tilt angle of 45°. Therefore, an altered tilt angle is the result of the depolarization in the material.
3) The third variable (d) represents the degree of polarization as discussed previously. The two polarization angles may also be altered by the geometry of the sample since a narrow ray as assumed in the previous evaluation can in the reality not approximate the transmitted beam.

III. Measurements

The polarization measurements were made with a vector network analyzer connected to a wide-band horn antenna. The optimal frequency band was determined to be 4–8 GHz, as the best

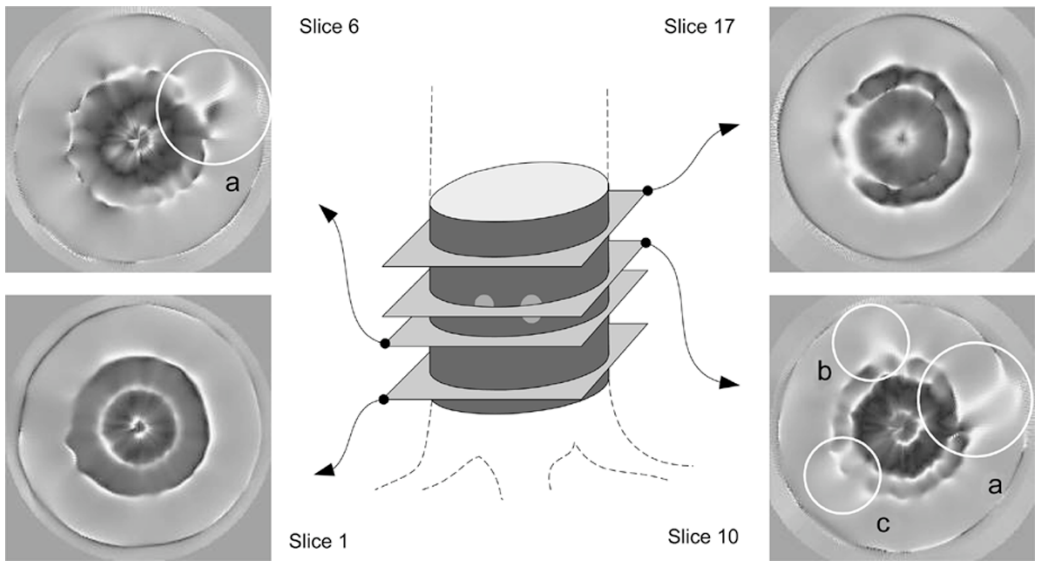

Fig. 9. Sequence of selected slice images representing the ellipticity angle ε.

response to contrast of fiber structure and artifacts and attenuation in the wood material.[1] A photo of the experimental setup is shown in Fig. 4.

The wood sample was mounted on a rotating conveyor, which allowed controlled rotation and translation of the sample. The object was rotated a full turn in two-degree steps. The sample was also moved lengthwise at one slice per centimeter. Each measurement resulted one-dimensional data along the radial direction of the object. The measured data was transformed into time-delay spectra and resampled on a rectilinear grid for visualization purposes.

Volume data sets were then created for the polarization ratio (30), the Stoke parameters (31), and the polarization angle (32).

IV. Results

The measurements described in this paper were all made on the same piece of spruce with dimensions of 175 mm in diameter and 180 mm in length. Fig. 5 describes the general outline of a horizontal slice through the log. The dark, numbered regions indicate the positions of knots inside the log.

Fig. 6 shows the Stoke parameters images of the same slice of the spruce log. These images show that each individual Stoke parameter intensity image is dominated by the very strong reflection at the surface of the log and that the contrast therefore is not sufficient to distinguish the variations inside the log. However, from our discussion above, we would expect these images to indicate the variation in moisture content in the log. The seemingly lack of contrast, therefore, indicates that the moisture content is a slowly varying parameter in the log.

Fig. 7 shows the complex polarization ratio as amplitude and phase angle of the same slice of spruce. Artifacts of the inner structure are apparent, especially the radial artifacts corresponding to the positions of the knots in Fig. 5. These images represent, according to our discussion above, mainly the variation in moisture and density of fiber inside the register. It can be noted that the border between sapwood and heartwood is clearly indicated in these images.

Fig. 8 shows images of the two polarization angles, elliptical and linear tilt angles, of the same slice of spruce. These images clearly show the most contrast where the fiber structure change and that all knots are distinguishable. This result is as expected since the two angles represent the fiber angle along the line of sight of the beam (ellipticity angle ϵ) and the fiber angle in the longitudinal-tangential plane (linear tilt angle τ).

V. Discussion

The ability to follow a knot in a sequence of slice images, captured along a trunk, is demonstrated in Fig. 9. The slices chosen from the sample show the spatial variations in the ellipticity angle. The two end slices (1 and 17) do not show any artifacts that can be interpreted as knots which is also expected due to the absence of knots in these regions. The other two slices from the mid part of the log sample are chosen to show the slice at the location where the knots are visible on the surface (slice 10) and slightly below the knot toward the ground (slice 6). Slice 10 also corresponds to the knot map in Fig. 5 and contains four knots. The circles marked with (a) correspond to the knots on the drawing of the sample and to knots 1 and 2 in the knot map in Fig. 5. The remaining two circles (b and c) mark the knots that are not visible on the front side of the log and correspond to the knots 3 and 4 in the knot map.

The polarimetric measurements have here been shown to be capable of producing images that reveal the locations and orientations of knots in a tree. This is in contrast to imaging based on the intensity that is only capable to show knots resulting from large branches. The penetration depth is in the order of 10% or less of the trunk diameter and, thus, the intensity will not deliver much information by itself of the relatively weak reflections from the inner parts of the tree . In contrast, the state of

[1]The bandwidth is needed to resolve close objects while the upper limit is determined by the attenuation in wood and the lower limit is determined by the spatial dimensions of the obstacles

polarization, which is based on the ratio between the field components and the phase shifts between the components, is capable of revealing information at deeper depths.

The slice images in Figs. 7 and 8 show that it is possible to locate knots using polarization data. These examples show that variations in the fiber structure do affect the polarization so that knots can be revealed in cases where the intensity images does not reveal more than the front surface reflection of the trunk.

The effort in future work can be divided into three categories which, to some extent, overlap each other.

1) *Reconstruction:* The performance of the reconstruction of the slice images can be improved in two ways: by increasing the precision and robustness and by reducing the processing time to real time performance (see, e.g., [16] and [17]).
2) *Segmentation:* The task of the segmentation is first to identify anatomical parts of the tree, such as knots or the interface between sapwood and heartwood.
3) *Estimation:* A further step of the reconstruction is to relate the optical parameters to wood physics parameters, such as moisture content, density, and fiber angle.

Another application besides locating knots in the trunk is to diagnose trees *in vivo* regarding fungal attacks and cavities. The variations in the dielectric matrix do as previously mentioned also vary with density and moisture content. These variations can be used as indicators to find decay and cavities in the trunk. In the early stages of a fungal attack, the moisture content will locally increase in the diseased region while the density decreases. These changes will increase the dielectric axial ratio $(\epsilon_L/\epsilon_{RT})$, and the corresponding change of the ellipticity angle will result under these conditions in a larger image contrast at the surface of the attacked region.

VI. Conclusion

We conclude, based on our results described in this article, that it is possible to study the variations in fiber structure, as well as density and moisture content in wood, by way of microwave radar tomography. Informative, three-dimensional images of the inside of a log can be made based on the microwave polarization variations.

The technology to build microwave tomographic scanners for fiber material at industrial scales is, therefore, at hand. We suggest that these can be built at low prices, work at very low power to be safe for humans, and, therefore, are commonly available.

Further research will concentrate on faster reconstruction algorithms and automatic segmenting of images, while technical development will concentrate on the production of generally affordable microwave tomographic systems.

References

[1] D. L. Schmoldt, J. C. Duke, M. Morrone, and C. M. Jennings, "Application of ultrasound nondestructive evaluation to grading pallet parts," in *Proc. 9th Int. Symp. Non-Destructive Testing of Wood*, 1994, pp. 183–190.

[2] S. C. Lee, J. Chen, and D. A. Hay, "Scanning logs for knots," in *Proc. 7th Scandinavian Conf. Image Analysis*, 1991, pp. 513–520.

[3] I. Svalbe, S. Som, J. Grant, J. Davis, K. Tsui, and P. Wells, "Internal scanning of logs for grade evaluation and defect location," in *Proc. 2nd Int. Workshop on Scanning Technology and Image Processing on Wood*, 1995, pp. 1–8.

[4] D. Zhu, R. W. Conners, D. L. Schmoldt, and P. A. Araman, "A prototype vision system for analysing CT imagery of hardwood logs," *IEEE Trans. Syst., Man, Cybern. B*, vol. 26, no. 3, pp. 522–532, Jun. 1996.

[5] J. Oja and E. Temnerud, "The appearence of resign pockets in CT-images of norway spruce (Picea abies (L.) karst.)," *Holz als Roh- und Werkstoff*, vol. 57, pp. 400–406, 1999.

[6] D. Choffel, P. Martin, B. Goy, and D. Gapp, "Interaction between wood and microwaves automatic grading application," in *Proc. Workshop on Scanning Technology and Image Processing on Wood*, 1992, pp. 1–8.

[7] R. J. King, "Microwave electromagnetic nondestructive testing of wood," in *Proc. Non-Destructive Testing on Wood*, 1978, pp. 121–134.

[8] J. B. Forrer and J. W. Funck, "Dielectric properties of defects on wood surfaces," *Holz als Roh- und Werkstoff*, vol. 56, no. 1, pp. 25–29, 1998.

[9] W. L. James, Y.-H. Yen, and R. J. King, "A microwave method for measuring moisture content, density, and grain angle of wood," USDA Forest Service Res. Note FPL-0250, 1985.

[10] M. Tiuri, K. Jokela, and S. Heikkelä, "Microwave instrument for accurate moisture and density measurement of timber," *J. Microw. Power*, vol. 15, no. 4, pp. 251–254, 1980.

[11] M. I. Belenkii and B. Z. Taibin, "On determination of the moisture content of wood," *Radiophys. Quantum Electron.*, vol. 37, no. 4, pp. 329–331, 1994.

[12] J. Shen, G. Schajer, and R. Parker, "Theory and practice in measuring wood grain angle using microwaves," *IEEE Trans. Instrum. Meas.*, vol. 43, no. 6, pp. 803–809, Dec. 1994.

[13] G. Kristensson, *Elektromagnetisk vågutbredning* . Lund, Sweden: Studentlitteratur, 1999.

[14] M. Norimoto, "Dielectric properties of wood," *Wood Res.*, vol. 59/60, pp. 106–152, 1976.

[15] G. I. Torgovnikov, *Dielectric Properties of Wood and Wood-Based Materials*. New York: Springer-Verlag, 1993.

[16] T. J. Cui, C. H. Liang, and W. Wiesbeck, "Closed-form solutions for one-dimensional inhomogeneous anisotropic medium in a special case—Part I: Direct scattering problem," *IEEE Trans. Antennas Propagat.*, vol. 45, no. 6, pp. 936–941, Jun. 1997.

[17] ——, "Closed-form solutions for one-dimensional inhomogeneous anisotropic medium in a special case—part II: Inverse scattering problem," *IEEE Trans. Antennas Propagat.*, vol. 45, no. 6, pp. 942–948, Jun. 1997.

Anders P. Kaestner was born 1971 in Helsingborg, Sweden. He received the M.Sc. degree in computer systems engineering with specialization in mechatronical systems from Halmstad University, Halmstad, Sweden, and the Ph.D. degree from the Chalmers University of Technology, Gothenburg, Sweden, in 1997 and 2002, respectively.

Currently, he is with the Swiss Federal Institute of Technology, Zurich, Switzerland, as a postdoctorate with the Institute of Terrestrial Ecology.

Lars B. Bååth was born 1948 in Kalmar, Sweden. He received the Ph.D. degree from the Chalmers University of Technology, Gothenburg, Sweden, in 1980.

He is currently a Professor of photonics at Halmstad University, Halmstad, Sweden.